Numerical Simulations of Wind-Loaded Floating Solar Panels

Andrea Mignone (a), Gabriele Inghirami (b), Francesco Rubini (c), Raniero Cazzaniga (d), Monica Cicu (d), Marco Rosa-Clot (d)
(a)Department of Physics, Turin, Italy
(b) University of Jyväskylä, Department of Physics, P.O. Box 35, FI-40014 University of Jyväskylä, Finland and Helsinki Institute of Physics, P.O. Box 64, FI-00014 University of Helsinki, Finland
(c) Department of Physics and Astronomy, Florence, Italy,
(d) Koiné Multimedia Via Alfredo Catalani 33 56125 Pisa, Italy

1. Introduction

Energy production from photovoltaics (PV) modules has been fast increasing in the last ten years and in 2019 has reached the value of 720 TWh worldwide. More recently the PV energy has been flanked by the birth of a new sector, the floating PV (FPV) technology. In both cases, the structures deployed on vast surfaces of land or water are designed to last 20 years in any weather conditions. However, the stability of these structures has been severely tested by external agents and in particular by gusts of wind that can lead to the plant breakdown. See Figure 1.

Figure 1 Effect of wind gusts on PV Modules positioned on a set of canopies (left) and an FPV plant (right)

For these reasons several studies have been done to understand the behavior of these structures and in particular the drag forces acting on the arrays: these studies have been done using CFD simulation programs or, in some cases, testing scale models in wind tunnels (see for example [1], [2] and reference therein). In a recent paper an analysis of the problem has been given, resulting in a closed-form formula to evaluate the drag forces. The CFD results have been compared with in-scale wind tunnel test applied to gable structures [3].
In this paper, we concentrate our attention on a specific FPV solution, the gable structure, defined in reference [4], see Figure 2

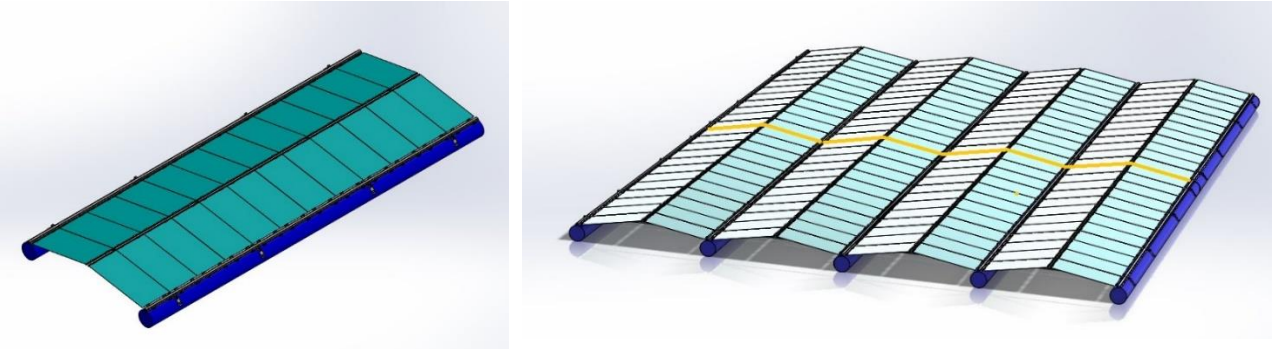

Figure 2 Gable structure, single raft (left) and set of 8 rafts (right)

Each raft has 24 PV modules on top of a simple canopy structure, the tilt angle is 10°. PV modules size is 2x1 m and the raft dimension is about 12x4 m.
This specific structure has been studied to resist strong winds and the raft equipped with PV modules has a rather large weight (1300 kg) and a suitable buoyancy (2400 kg).
Using this basic structure, we study the impact of wind with two different simulation tools:

1. The code **PLUTO**, developed by Andrea Mignone and collaborators, at the Department of Astrophysics of the University of Chicago, USA, and currently worldwide used for astrophysical purposes involving classic and relativistic low-density plasmas in stars and the interstellar medium. [5]
2. **Flow Simulation** is a full analysis Computational Fluid Dynamics (CFD) software to simulate liquid and gas flow

Up to now Code PLUTO has been used for low-density plasma astrophysics problems. In this paper, we extend its application by using air in standard condition as a compressible flow and imposing specific boundary conditions. The comparison of two CFD applications that were originally developed for the study of different environments is particularly interesting in evaluating the results. Although tests have already been carried out using air in standard condition to check the code reliability (see the Double-Mach Reflection or the Rayleigh-Taylor and Kelvin-Helmoltz instabilities), it is the first time that the code investigates the aerodynamics of a solid body. The comparison with the results of the Flow3D code reveals differences that are still under investigation. The expected convergence between the two codes would certify a powerful and self-produced numerical tool, specially tailored for studying the aerodynamics of solar panels installations in any kind of geometry and atmospheric conditions.
The two codes are used to study a 2D problem described in Figure 3 with the wind coming from the left and impinging on the regular structure of 5 gable rafts. Each raft is constituted by a double set of PV modules of 1.5x1 m and is in contact with the neighbouring raft.

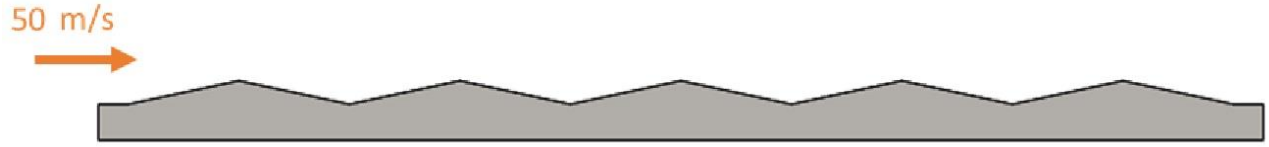

Figure 3 Schematic structure used in the 2d simulation tests

Two cases are discussed with strong wind conditions: 50 m/s (Case A) and 35 m/s (Case B).
The wind is assumed to be parallel to the water surface and is used as a constant steady input. (in the PLUTO simulation the case of wind impinging with a direction of 30° will also be studied). Reality is quite different and normally wind is measured at the height of 10 m and varies with the quota according to the empirical power-law parametrization, called Hellman law.

$$v(z) = v(z=10\ m)\ (z/10)^{\alpha} \qquad \text{Eq. 1}$$

Then, assuming the low value $\alpha = 0.1$, our simulation will be for the effective wind of 44 and 64 m/s that is 160 km/h and 225 km/h respectively. Note that this simulation uses a constant wind velocity without the natural turbulence usually found in real world wind conditions which lead to varying wind speeds/gusts; so a direct comparison with wind speeds measured in the real world cannot directly be made although the constant wind speed can be considered similar to a very short duration constant velocity gust applied over the whole structure.
Using these input initial conditions, we solve the equations of ideal hydrodynamics in conservative form,

$$\partial\rho\ \partial t + \nabla\cdot(\rho v) = 0, \qquad \text{Eq. 2}$$
$$\partial\rho v\ \partial t + \nabla\cdot[\rho vv + Ip]| = 0, \qquad \text{Eq. 3}$$
$$\partial E\ \partial t + \nabla\cdot[(E + p)v] = 0 \qquad \text{Eq. 4}$$

Here ρ, $v = (v_x, v_y)$ and p are used to denote the mass density, velocity, and thermal pressure. The total energy is defined by the sum of thermal and kinetic contributions,

$$E = \rho e + 1/2\ \rho v^2 \qquad \text{Eq. 5}$$

where, using an adiabatic equation of state, $\rho e = p/(\gamma - 1)$, with $\gamma = 1.4$ being the specific heat ratio for air. The hydrodynamic equations are solved on a 2D Cartesian domain defined by $x \in [0,30]$ m and $y \in [0,12]$ m.
Our initial condition consists of a uniform medium with constant pressure $p = cs^2\rho/\gamma$ where cs = 340 m/s is the adiabatic speed of sound in the air while $\rho \approx 1.231 Kg/m^3$ has been chosen so that p = 101,325 Pa.
We initialize the domain with a constant velocity field v_{in} parallel to the x-axis. On the left and on upper boundaries, we adopt inflow boundary conditions by keeping boundary values equal to the initial conditions. At the lower boundary (y = 0) we assign reflective conditions, while at the highest boundary values in the ghost zones are copied from the last active zones (zero gradient).

2. Code PLUTO and the numerical simulation.

Eq. 2-4 are solved using the PLUTO code for astrophysical gas-dynamics, which uses adaptive mesh refinement. The code employs a finite-volume Godunov-type approach to solve hyperbolic conservation laws of different kinds, ranging from hydrodynamics to relativistic magneto-hydrodynamic, including also non-ideal effects such as viscosity, thermal conduction, and resistivity [6], [7], [8]. For simplicity, these terms have not been added to the current work. The numerical approach heavily relies on the solution of Riemann problems between discontinuous states at zone interfaces. Left and right states are typically produced using a high-order oscillation free reconstruction technique [9]. For the present paper, we use a characteristic tracing algorithm to achieve second-order accuracy in time and a parabolic reconstruction based on the original PPM method to reconstruct characteristic variables inside each zone. In our simulations, we employ the HLLC Riemann solver [10].
The presence of solid bodies has been imposed by first identifying computational zones that fall inside a user-defined physical region. The solution is not evaluated in these cells which, on the contrary, are used to provide symmetric (for scalar quantities or transverse velocity components) or antisymmetric (for normal velocity components) profiles to mimic a reflective wall at the solid-gas

interfaces. In order to reduce the stair-case representation of solid bodies, we concentrate mesh refinement at solid-gas interfaces. The base grid consists of 320×128 zones, and 4 levels of refinement are employed thus yielding an equivalent resolution of 5120×2048 zones. It's worthwhile to underline that the used mesh yields a numerical error of the order $\approx 10^4 - 10^5$ suitable to introduce approximation in the pressure evaluation of the order 10-100 Pa. As a consequence, the preliminary results shown here should be considered as a rough estimate of the real values. In order to achieve the exact number for loads, a much higher resolution should be used, which is the goal of the next improved simulations.

All simulations start at time t=0 s and end at time t=5 s. The floating platform has been schematized with a sequence of ten panels, alternatively upwind and downwind with respect to the wind direction, flowing from the left to the right (Figure 3). The first upwind panel is labeled as panel number 1, the last, downwind panel is panel number 10. Results are shown in the following figures. The effect of such interaction, in terms of panel-load is shown in the next figures. Since simulations have been run in 2 dimensions, this means that a platform 1 meter large in the third, unresolved dimension, has been assumed.

- Figure 4 describes the time behaviour of pressure and vorticity on the full system
- Figure 5A. The two pics at the top represent, respectively, the horizontal and the vertical component of the total load on all the panels (picture on the left) and the loads on the left and right float (picture on the right) for Case A, (v=50 m/s). Loads are plotted as functions of time. The two pictures at the bottom show the time-averaged horizontal and vertical loads on each panel.
- Figure 5B. Same as 5A for Case B (v=35 m/s)
- Figure 6A. Comparison between loads on the first and last upwind and downwind panel, respectively, Case A.
- Figure 6B. Same as 6A for Case B.

In order to calculate the forces acting on the panels, we have used the pressure gradient criterium. The forces due to the pressure gradient inside cells of gas neighboring the panels have been computed: since panels are internal, reflecting boundaries, such forces are also exchanged between gas and panels.

The total load has been computed summing up the forces acting on each panel and neglecting the component due to the lateral floats, that have been considered separately. Both the horizontal (red line) and the vertical load (green line) are almost stationary functions, fluctuating around average values.

The horizontal load is quite small in both 50 m/s and 35 m/s case and, on average, is directed rightward, following the wind direction.

The vertical component is much more important and is directed downward, meaning that the wind pushes on the panels from above. Once again, the calculated numbers should be taken carefully because of the numerical error affecting the pressure field though, since the small values are in the error range, higher loads are not expected. The lateral floats have been considered separately in figures 5A) and 5B), which show the total horizontal force on the float at the left (red line) and right side of the platform (green line) in the two cases. The two plots look quite different.

The wind interacting with the left float forms a stationary over-pressured region of gas close to the vertical surface, that applies an almost steady, rightward directed force to the float, whose time-averaged value is, in case A, about 8 times case B.

On the right side, instead, the wind streamlines keep the panel's shape even to the right of the left float, according to the so-called Kamm's effect.

As a consequence, a bubble of unperturbed gas with atmospheric pressure survives close to the float's surface, surrounded by lower pressure, high-velocity streamlines of wind, yielding a resulting leftward directed force whose average value is, in case A, about three times case B.
Fluctuations shown by the green line correspond to the fact that the over-pressured bubble of gas continuously undergoes compression and decompression by the surrounding, fast velocity wind, which yields a highly time-varying behavior. Of course, the Kamm's effect, arising from the truncated, vertical shape of the float, is expected to vanish if the floats were given cylindrical shape.

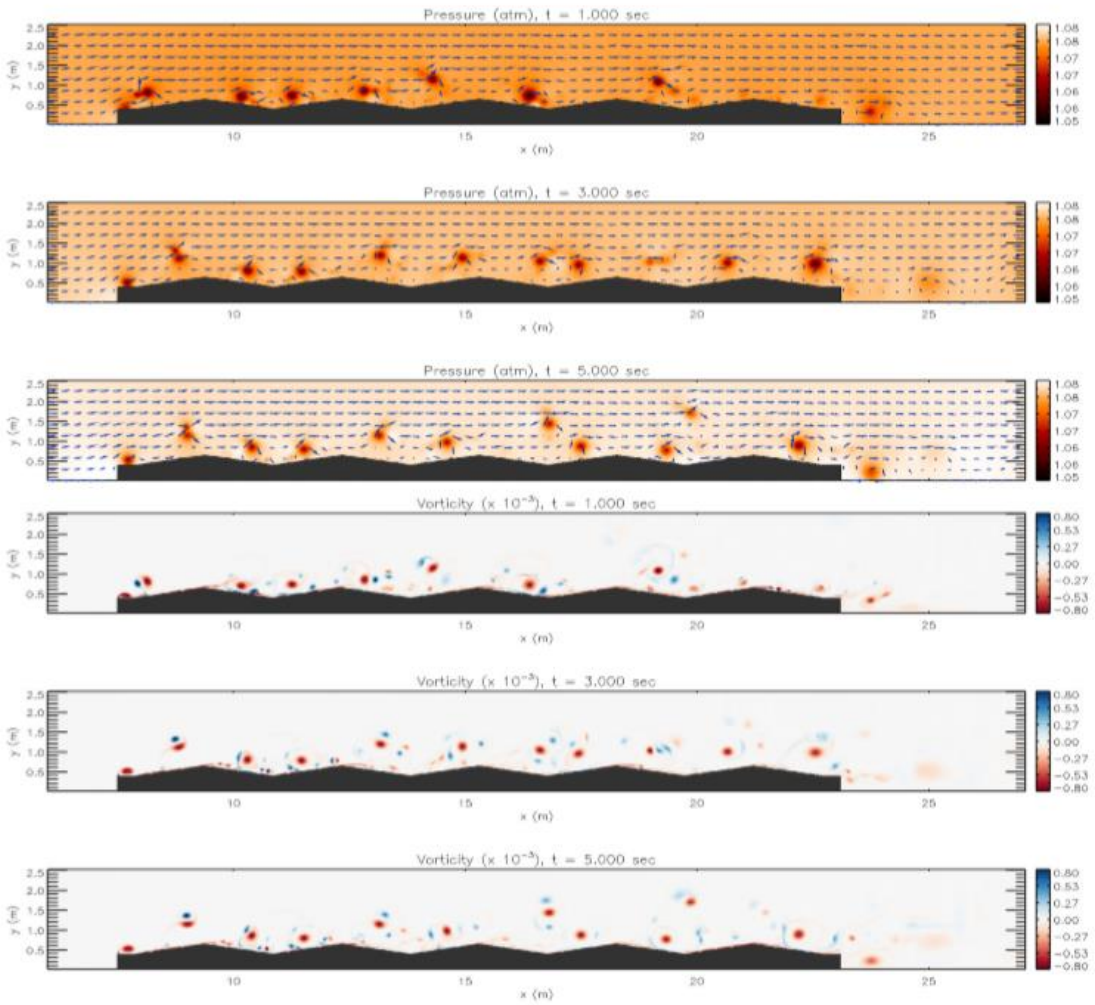

Figure 4: Pressure and vorticity fields at 3 different times 1, 3, 5 s for wind at 50 m/s

The pictures at the bottom of figures 5A) and 5B) show the time-averaged horizontal (left) and vertical (right) load, panel by panel. The horizontal component is rightward oriented for almost all the panels and is negligible with respect to the vertical, downward component. Both for the horizontal and vertical component, the panels numbered from 1 to 5, covering the left half of the platform, experience higher loads with respect to panels numbered from 6 to 10. It is worthwhile to notice that the average load on panel number 2, the first downwind panel, is higher than the load on panel number 1, the first upwind panel, because of the shielding effect provided by the float.
Figure 5 at the top-left shows both the horizontal and vertical component of the total load, acting on the whole structure, as a function of time. At the top-right, the horizontal loads on the floats, schematically represented as vertical surfaces, have been plotted. Plots at the bottom show the time-averaged horizontal and vertical loads on each panel.
Plots at the bottom show the time-averaged horizontal and vertical loads on the ten panels.

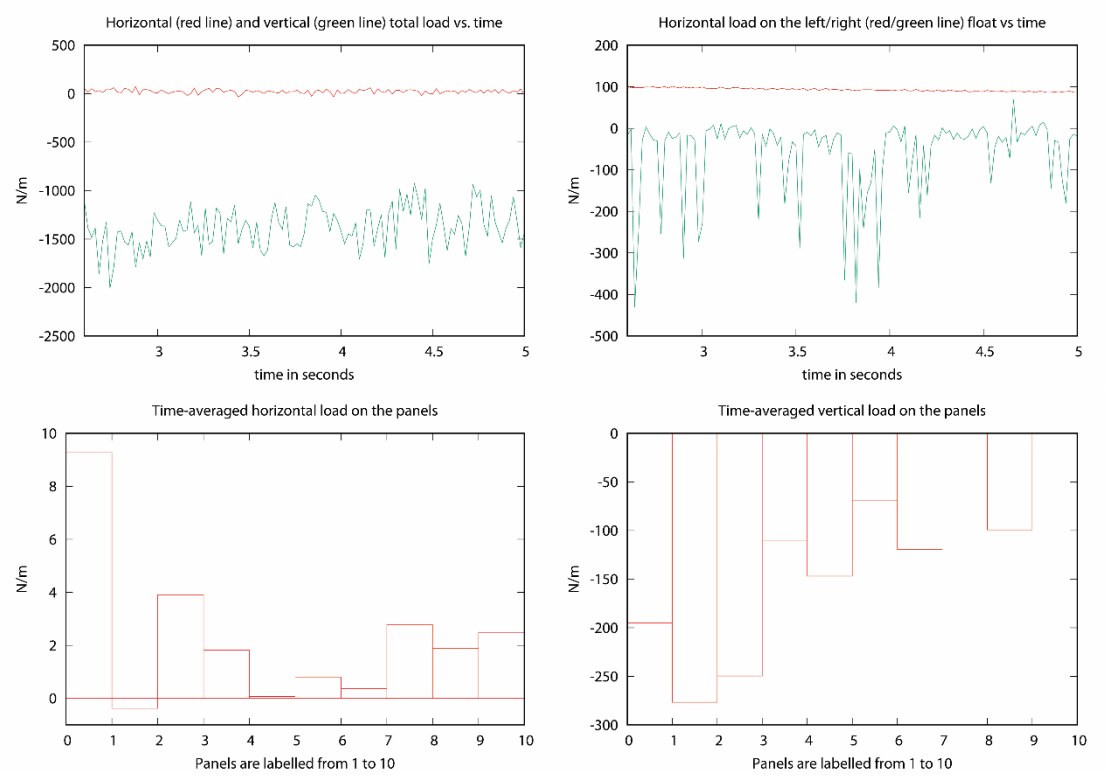

Figure 5 Horizontal and vertical load. Case A 50 m/s (left)

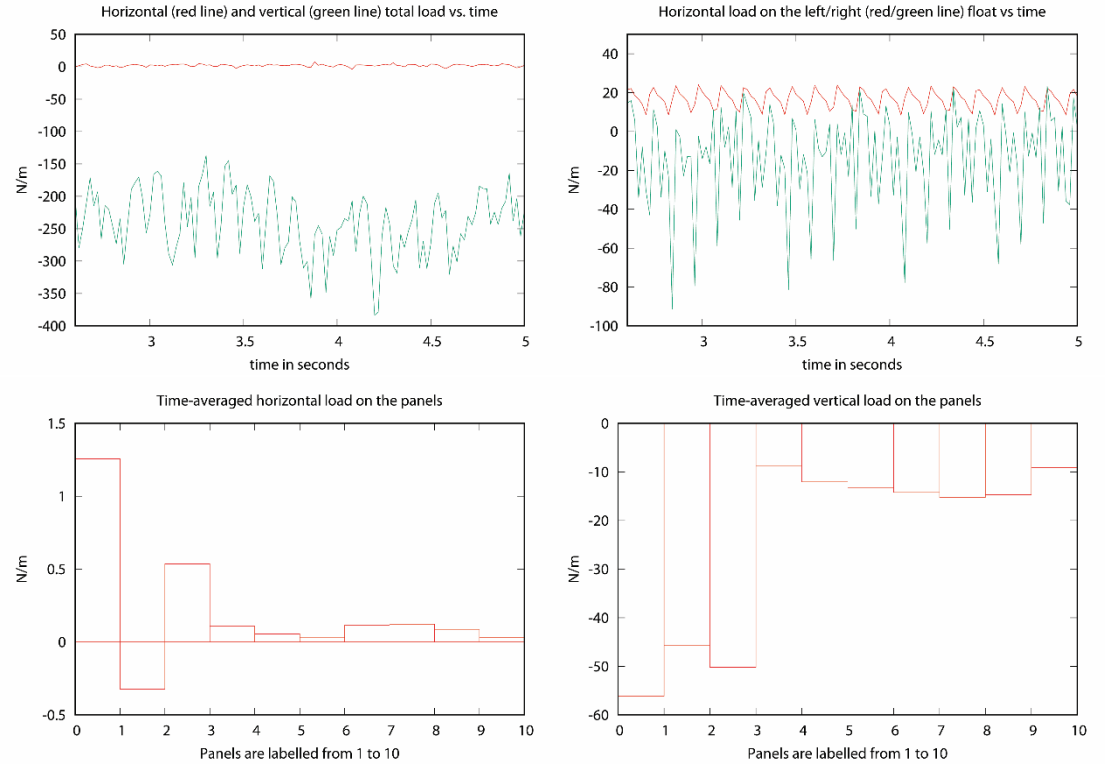

Figure 6 Horizontal and vertical load. Case B 35 m/s (right)

Figure 7 shows that the load on the first couple of panels is stronger than the load on the last one, though the difference is higher in downwind panels, since panel number 2, the first downwind panel, undergoes the highest load.

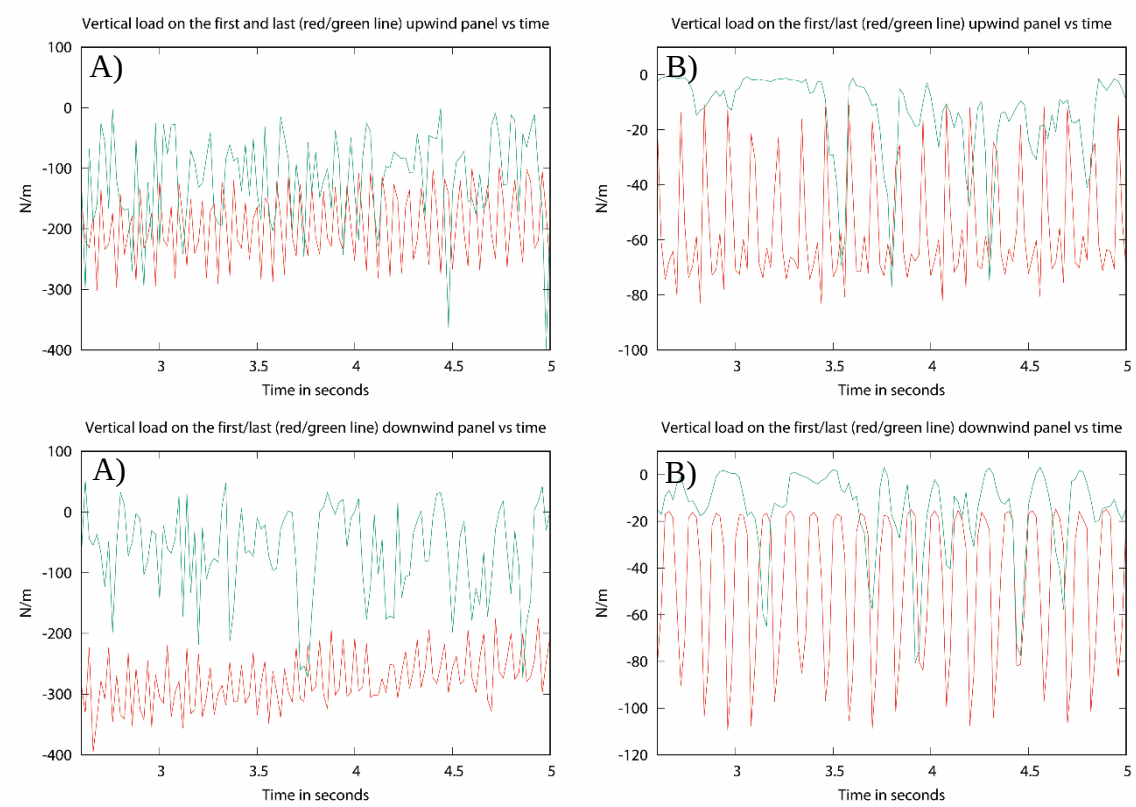

Figure 7 The vertical load vs time on the first (red line) and last (green line) upwind (top) and downwind (bottom) panel; left for case A), right for case B).

All curves in this figure show high-frequency oscillations at about 15-20 Hz, which might be due to numerical rather than physical effects, namely, from the propagation of the sound waves allowed by the compressible model used for the gas. In our opinion, such oscillations could be removed by some interpolating techniques. Case B qualitatively reproduces the same features of Case A, though with weaker loads.

The most relevant difference between results from code PLUTO and Flow Simulation is that the former does not show the stationary pattern of the latter. Figure 4, in particular, reveals the unsteady, turbulent pattern in both velocity and pressure field, which affects the computed loads. In particular, PLUTO simulations do not show the stationary low-pressure regions that correspond to the pinnacles connecting upwind and downwind panels, which is strong enough to lift panel number 1 (see next figures).

In order to investigate such a different behaviour, 3D simulations need to be performed, since it is well known that 2D turbulence is likely to show unrealistic effects.

3. Flow simulation: 2D analysis

The simulation has been done using the same schematic profile as PLUTO and given in Figure 1 7-11 . The main parameters of the simulation are described in the table below.

Table 1 Domain dimensions and mesh characteristics

X min	-1.000 m	Total Cell count:	808532
X max	16.000 m	Fluid Cells:	808532
Y min	0 m	Solid Cells:	1928391

Y max	3.000 m	Partial Cells:	238752
Z min	0 m	Trimmed Cells:	0
Z max	1.000 m	Total Cell count:	808532
Number of cells in X	2501		
Number of cells in Y	401		
Number of cells in Z	1		

Results for pressure and turbulence length are given in Figure 8 and Figure 9.

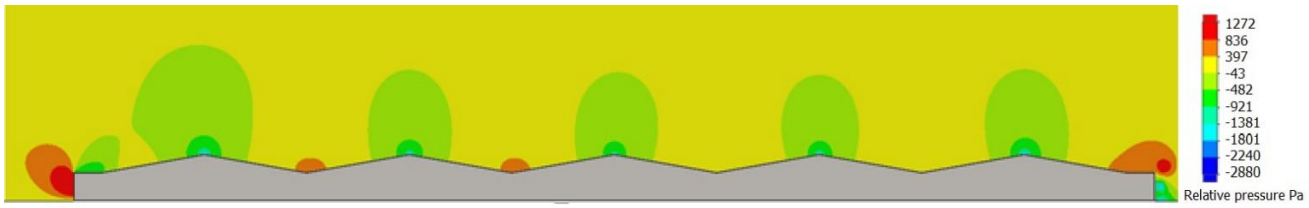

Figure 8 Pressure plot for 50 m/s

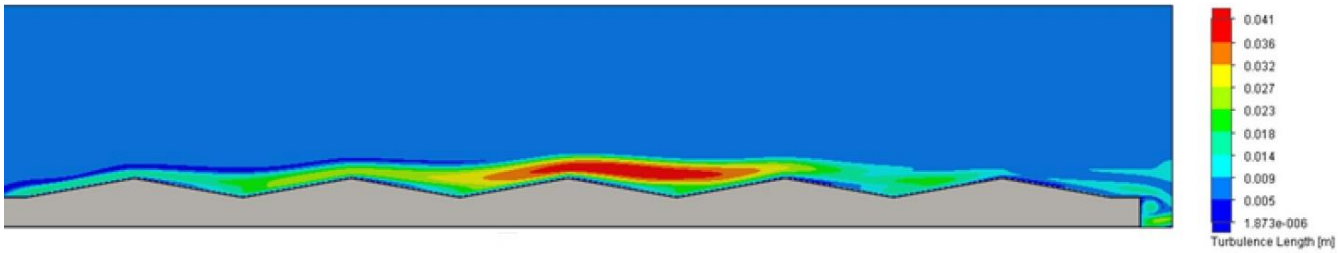

Figure 9 Turbulence length

These plots highlight the depression on the top of the gable structures and the strong pressure on the left vertical float and a lower but always positive pressure on the right vertical float. The value of the forces acting on this vertical barrier depends critically on the detailed shape of the structure. Relative pressure is given in Figure 10 and plotted explicitly in Figure 11

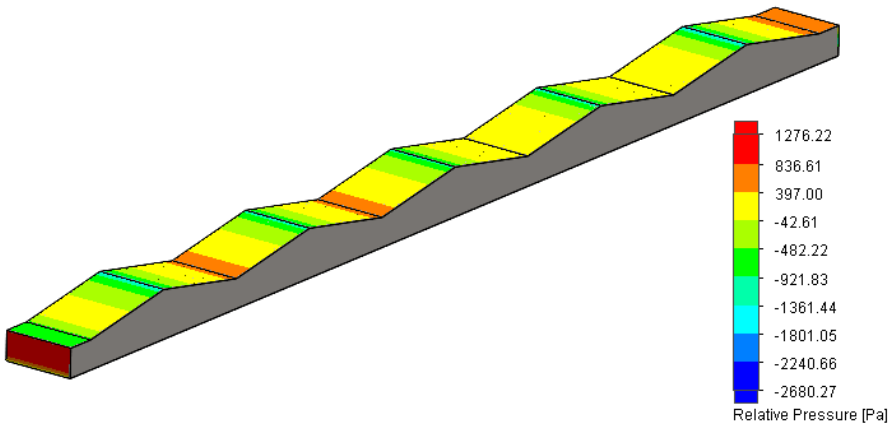

Figure 10 Relative pressure

All these three plots agree qualitatively with results obtained by PLUTO code, the main differences being due to the different representation: PLUTO shows the temporal behaviour of the physical parameters, whereas Flow3D shows the average result of the same quantities. We get analogous plots in the 35 m/s case.

In order to better understand the lift and load mechanism, we give here below the relative pressure value along with the rafts profile for the two wind speeds.

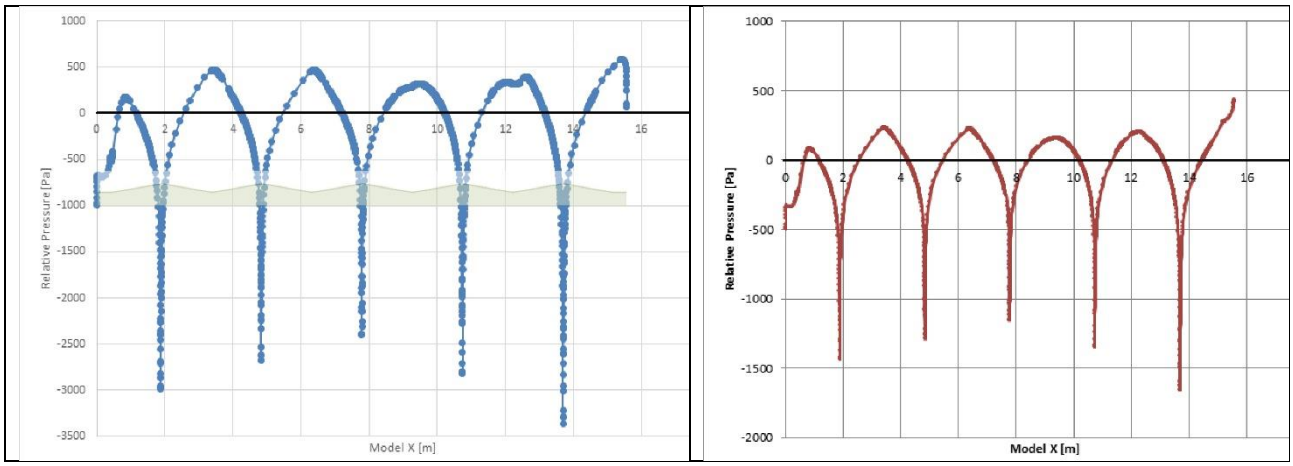

Figure 11 XY plot – relative pressure : left 50 m/s (blue) right 35 m/s (red)

The strong lift effect at the top of the gables and the positive pressure in the valleys between two adjacent gables are quite evident. The full vertical pressure is the result of these two opposite effects and is shown in Figure 12 both for x and y forces components.

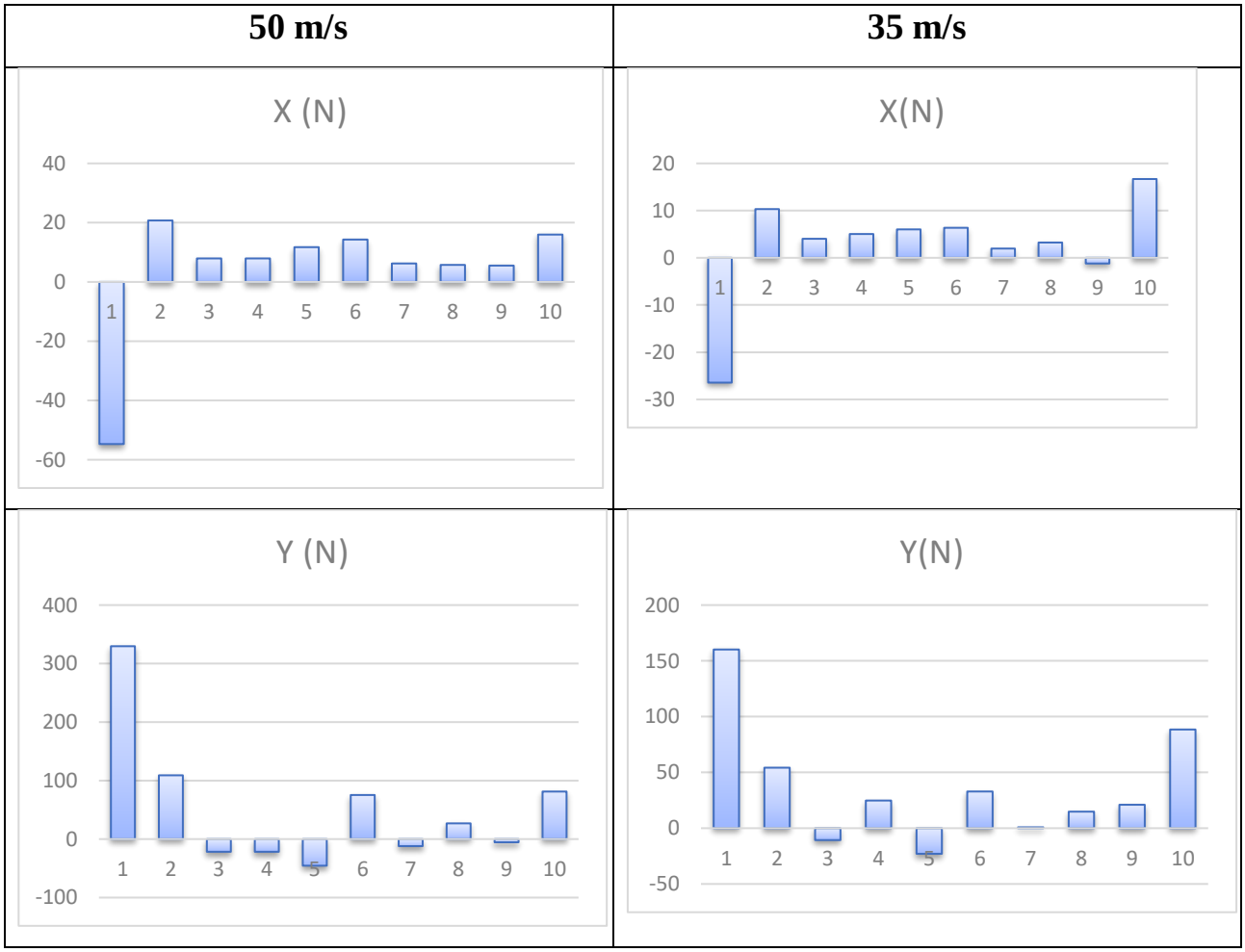

Figure 12 Plots of the forces (horizontal -X(n)- and vertical -Y(N-) acting on the 10 PV modules. Note the different scales on the right histograms.

It is interesting to see that there is a scale reduction of a factor $(35/50)^2 = 2.04$ which is quite evident for the forces along x. The same thing happens for the forces along y in the first 2 modules and the last one. The strong compensation of positive and negative forces on the other modules gives a rather irregular behaviour. The same scale factor is found for global horizontal drag as shown in the following table.
In Table 2 the global forces on the structure are given.

Table 2 Global forces on the structure

Name	Unit	50 m/s	35 m/s
GG Force (X)	N	860	331
GG Force (Y)	N	628	366
Horizontal load on Left vertical floats	N	537	260
Horizontal load on Right vertical float	N	280	45
Drag Factor Cd		0.85	0.66

The drag factor is obtained from the equation

$$C_d = \frac{2\, GGForce(x)}{\rho v^2 S} \qquad \textbf{Eq. 6}$$

where S is the structure cross section in m^2.
It's worth noting that the two floats play an important part on the previous result but in any case, forces are of few hundreds N and should be compared with the gravity forces (raft mass is 1300 kg) and buoyancy (2400 kg). This means that, even taking into account the temporal fluctuation described in the PLUTO code, the gable structure, subjected to a wind of 50 m/s (180 km/h at the water level that is 225 km/h at the standard level of 10 m), is essentially stable.

4. Comparison of the two different approaches and conclusions

The results of the two codes are in a qualitative agreement and show velocity fields and turbulences quite similar and comparable. The wind load calculations however are quite delicate and depend on pressure variation, which is typically 100 Pa, that is 0.1% of the average pressure acting on the system so that small corrections can be important. Because of the available time, the precision of the codes is not sufficient and it was not possible to increase the mesh dimension in order to get more accurate result: so, for example, the action on the first module windward is positive in the PLUTO code and negative in the Flow code. However, a common result is that the wind load on the inner modules is strongly reduced by about one order of magnitude and that of course the impact of the wind on the initial wall is strongly positive and gives rise to a global drag from left to right.
This is in contrast with what emerges from a rough analysis which suggests $w_e = c_d \tfrac{1}{2} \rho\, v^2 = 0.8\, v^2$ for m^2 which generates higher values. Furthermore, a frequently used thumb rule is that the wind load on the gable structure after the first panel is reduced by one third whereas in our case the reduction is stronger.
Therefore the most important results in both approaches are that the force along X increases with the raft's number but with a contribution from the internal rafts which is much lower than that of

the first one. Furthermore, forces along Y are two orders of magnitude less than the gravity and buoyancy ones, respectively 13000 N and 24000 N.
This first model, chosen for its structure, is completely solid and because of that, the gaps, between pipes and structure, and the gaps between different parts of the structure itself, are not represented. Another aspect that is not analysed here is the back of the panels where we expect to find pressures in-phase and reversed-phase with respect to the ones on the top. A subsequent 3D analysis will take into account all these aspects to refine the study.
Further work is in progress: PLUTO will extend the analysis to a refined mesh and over a longer time. A further calculation will be performed with wind impact with a Z component and, eventually, a 3D simulation will allow the extension of the simulation to a more precise form of the gable structure.
Flow Simulation will be applied to a 3D case studying the wind load when the array is hit by wind parallel to water surface but with impact angles different from zero. In the end, the plant will be described taking into account a detailed drawing and using semi immerged round pipes (and not a vertical step) as supporting structure.

5. Acknowledgments

We thank Michele Calì, Electric, Electronics and Computer Engineering Department, University of Catania E-mail: michele.cali@dieei.unict.it and the engineering department of Catania for providing us with the use of the code FlowSimulation.

6. References

[1] O. Bogdan and D. Cretu, “Wind Load design of phtovoltaic power plants by comparison of design codes and wind tunnel tests,” *Mathematical Modelling in Civil Engineering*, vol. 15, no. 3, 2019.

[2] I. Sheikh, “Numerical Investigation of Drag and Lift Coefficient on a Fixed Tilt Ground Mounted Photovoltaic Module System over Inclined Terrain,” *International Journal of Fluids Engineering*, vol. 11, no. 1, pp. 37-49, 2019.

[3] P. Siribodhi and P. Bunyawanichakul, “Study and Evaluation of a Solar Floating Traction under Severe Wind Conditions,” in *Southeast Asia Workshop on Aerospace Engineering (SAWAE)*, 2019.

[4] M. Rosa-Clot and G. Tina, Floating PV Plants, London: Academic press, 2020 February.

[5] A. Mignone, F. Bodo, S. Massaglia, T. Matsakos, O. Tesileanu, C. Zanni and A. Ferrari, “PLUTO: A Numerical Code for Computational Astrophysics,” *Astrophysics*, vol. 170, pp. 228-242, 2007.

[6] P. Roe, “Approximate Riemann Solvers, Parameter Vectors, and Difference Schemes,,” *Journal of Computational Physics*, vol. 43, pp. 357-372, 1981.

[7] P. Colella, “Multidimensional upwind methods for hyperbolic conservation laws,” *Journal of Computational Physics*, vol. 87, pp. 171-200, 1990.

[8] B. van Leer, “Towards the ultimate conservative difference scheme. V - A second-order sequel to Godunov’s method,” *Journal of Computational Physics,* vol. 32, pp. 101-136, 1979.

[9] R. Borges, M. Carmona, B. Costa and W. Don, “An improved weighted essentially non-oscillatory scheme for hyperbolic conservation laws,” *Journal of Computational Physics ,* vol. 227, pp. 3191-3211, 2008.

[10] A. Mignone and G. Bod, “An HLLC Riemann solver for relativistic flows - I. Hydrodynamics,” *Monthly Notices of the Royal Astronomical Society,* vol. 364, pp. 126-136, 2005.